frontiers | Frontiers in Energy Research

TYPE Original Research
PUBLISHED 30 May 2024
DOI 10.3389/fenrg.2024.1335507

OPEN ACCESS

EDITED BY
Bengi Şanlı,
Mersin University, Türkiye

REVIEWED BY
Gökhan Tüccar,
Adana Science and Technology University, Türkiye
Wei Zuo,
Wuhan University of Science and Technology, China
Rajiv Kumar,
Birla Institute of Technology, India

*CORRESPONDENCE
E. E. Onojowho,
efe.elijah@gmail.com

†PRESENT ADDRESSES
E. E. Onojowho,
Department of Mechanical Engineering, University of Nigeria, Nsukka, Nigeria
A. A. Asere,
Department of Automobile Engineering, Elizade University Ilara-Mokin, Nsukka, Ilara-Mokin

RECEIVED 09 November 2023
ACCEPTED 02 April 2024
PUBLISHED 30 May 2024

CITATION
Onojowho EE and Asere AA (2024), Effects of the fuel blend flow rate on engine combustion performance.
Front. Energy Res. 12:1335507.
doi: 10.3389/fenrg.2024.1335507

Effects of the fuel blend flow rate on engine combustion performance

E. E. Onojowho †* and A. A. Asere†

Department of Mechanical Engineering, Thermo-Fluid and Energy Research Group, Obafemi Awolowo University, Ile-Ife, Nigeria

The aim of this study is to investigate the post-injection flow interactive effects of atomized fuel blends from an injector system of known characteristics into a direct injection compression ignition engine combustion chamber and their outcomes. Attempts were made to link the interactive influence of blend mixture quality, effluence and consumption rate of fuel injection properties on frictional loss, heat liberation, combustion, and volumetric efficiency performance outcomes of the engine. This numerical–experimental dimension study began with computational fluid dynamics (CFD) prediction of fuel in-cylinder behavior between a 225° CA (crank angle) (45°ABDC—after bottom dead center) and 360°CA (0° BTDC—before top dead center) compression stroke elapsing into an expansion stroke. A Testo gas analyzer was used to determine the combustion efficiency. The experiments validated the CFD outcomes presented. Willans lines were applied on blends to compare piston frictional losses. A swirl prediction maximum peak of 0.027237 at 336.15 CA for pure diesel blend (D_{100}) at 2,300 rpm and 0.066811 at 341.3 CA for pure biodiesel blend (B_{100}) at 1,800 rpm aided the mixing quality. The instantaneous velocity on the sinusoidal profile and contour around the swirling peak crank angle revealed ignition activity resulting from high mixing quality. The engine possessed high-efficient fuel blends burning strength on a minimum of 54.5% at a higher flow rate. The engine speed and flow rate interaction on the heat liberation rate made a symmetric profile for D_{100} and B_{100}. Engine energy loss on friction was minimal with D_{100} compared to B_{100} and 5% biodiesel to 95% diesel blend (B_5).

KEYWORDS

fuel flow rate, piston frictional losses, engine heat liberation rate, combustion efficiency, internal combustion engine numerical effluence

1 Introduction

Combustion is said to be a complex phenomenon of dependent factors. The internal combustion engine (ICE) system has gained significant research attention. Wysocki et al. (2018) introduced the technology of a mobile test rig on combustion, promoting the mobility of the performance and emission characterization site, even farm-based locations. Endoscope photographing technology in ICE fuel atomization and flame studies was applied by Mao et al. (2020) and Stepien et al. (2022), while the application of AI on pump and engine performance and emission and optimization studies were also presented (Karami et al., 2019; Ude et al., 2020; Onukwuli et al., 2021; Said et al., 2022; Yamin and Hdaib, 2022; Feng et al., 2023). A study on the mass flow rate effect found expression in

the thermal management of the battery fuel cell reaction phenomenon (Zuo et al., 2022). This strengthens the band of the electric vehicle clean power system in its use of the proton exchange membrane and its application and optimization in conjunction with hydrogen combustion technology in ICE (Zuo et al., 2023a; Zuo et al., 2023b; Chen et al., 2023; Zuo et al., 2023c).

Specific contributions of fuel combustion studies in engine performance and emission have been on a secondary and tertiary fuel blending ratio for spark ignition (SI) and compression ignition (CI) engines, as presented by Al-Hasan and Al-Momany (2008); Abdullah et al. (2015); Liu H. et al. (2015); Akar (2016); Deng et al. (2018); Mohammed et al. (2021); and Prasad and Saravanan (2021). The ternary fuel blending effect on pump was studied by Caligiuri et al., (2019). Also antioxidant and nanoparticles additives flow enhancement pay tribute to performance (Shahabuddin et al., 2013; Shaafi and Velraj, 2015; Feroskhan et al., 2017; Perumal Venkatesan et al., 2021; Daud et al., 2022; Küçükosman et al., 2022). Meanwhile, fuel spray and atomization, fuel injection timing, and pressure variation are current issues of study in the literature, as presented by Kumar and Rehman (2014); Liu J. et al. (2015); Rai et al. (2021); Sun et al. (2021); Küçükosman et al. (2022); Pham et al. (2022); and Stępień et al. (2022). The technique of dual-fuel engine mode with little or no adjustment of the engine system was studied by Feroskhan et al. (2017); Mahla et al. (2017); Ambarita, (2018); Parthasarathy et al. (2019); Estrada et al. (2022); and Jamrozik et al. (2022). To date, dual-fuel injection and combustion studies have focused on the gas fuel flow rate and mixing techniques of homogeneous charge compression ignition (HCCI) technology (Kumar and Rehman, 2014; Gnanamoorthi and Vimalananth, 2020; Atelge et al., 2022; Park et al., 2022; Zardoya et al., 2022). All these studies target the manipulation of fluid flow or its properties for investigating the effect on engine combustion and performance. Another significant addition to the aforementioned study is the impact of the flow rate either prior to or within the combustion chamber. Major works done so far focus on the variation in either fuel flow or air flow rates of various fuels accompanied with the blending effect on SI and CI engines. Mahla et al. (2017) and Parthasarathy et al. (2019) investigated the effect of compressed natural gas (CNG) flow rate variation on CI engine performance, while biogas and hydrogen flow rate variations were studied by others (Feroskhan et al., 2017; Ambarita, 2018; Estrada et al., 2022). Majority of the works focused on the flow rate, existing in the dual-fuel engine mode (Feroskhan et al., 2017; Mahla et al., 2017; Ambarita, 2018; Parthasarathy et al., 2019; Estrada et al., 2022) instead of the usual single-engine operation mode. In this regard, Jamrozik et al. (2022) stated the difference between the effect of both modes, i.e., the flame front will usually form around the injected stream and spread to the filled areas with a single engine; however, the limitations of fuel type will hinder this spread in a dual-fuel engine. Gnanamoorthi and Vimalananth (2020) concluded that the heat release rate (HRR), cylinder pressure, and NOx increased by 28.66%, 28.9%, and 7.3%, respectively, under 30 L/min of hydrogen fuel at brake power variation. A microscopic spray investigation discussed the effect of fuel physical properties and control parameters on atomization and submitted that the spray angle and droplet velocity depend on fuel viscosity (Sun et al., 2021). In another study, the effects of the spray droplet, ambient air mixing, and gas flow rate of a dual-fuel engine brake-specific fuel consumption (BSFC), in-cylinder pressure, and heat release rate improve, while brake thermal efficiency (BTE) and brake volumetric efficiency (BVE) generally remain lower compared to that when using traditional diesel (Pham et al., 2022). Furthermore, in a mixing study, the combination of an early pilot and a large squish piston geometrical approach on a natural gas–diesel dual-fuel engine was investigated using a double injection mode on engine BTE and emission. An improvement of 7.8% and 49.7% in BTE and methane emission, respectively, was obtained, which was better than that obtained with the single injection of pilot dual fuel (Park et al., 2022).

In-cylinder piston frictional mean effective pressure (FMEP) in ICE losses has been said to exist due to the collection of sub-frictional loses; mechanical mean effective pressure (MMEP) is applied to surmount mechanical friction; power-gaining mean effective pressure (PMEP) exists only in four-stroke engines; charging mean effective pressure (CMEP) is used in driving a supercharger or scavenging pump; turbine-added mean effective pressure (TMEP), turbine add-on pressure, and auxiliary-driving mean effective pressure (AMEP) are usually added with brake mean effective pressure (BMEP), thus yielding indicated mean effective pressure (IMEP) (Taylor, 1985b). Amid rundown, shutoff, Willans lines, motoring, strip, indicated and special measuring known methods of friction determination, according to Van Basshuysen and Schäfer (2004), the indicated method was applied in an experimental and simulation study of FMEP determination in a four-cylinder CI engine (Knauder et al., 2019). A similar study was executed numerically in a four-stroke four-cylinder SI engine, validating existing work (Mishra, 2013). The work suggested that an experimented frictional study by reason of higher boundary friction yields larger friction than the predicted friction. Second, frictional force is maximum within compression and power strokes and negligible in suction and exhaust strokes. Feng et al. (2022) presented a comparative study on energy balance on an automated and manual transmission hybrid vehicle to account for energy losses.

Researchers have also focused on the experimental and numerical dimensions of ICE flow. Increasing diesel and air flow rates in flame stability, combustion efficiency, and other parameters increased the combustion flame instability and efficiency (Li et al., 2022). An engine was studied as a two-phase flow-accommodating entity for heat and fluid flow in CFD studies of velocity magnitude, penetration length, swirl and tumble ratios, and heat release rate, and an experimented heat flow characteristic in blends of 100% pure *Khaya senegalensis* biodiesel blend (B_{100}), B_{20}, and pure diesel blend (D_{100}) of *Jatropha* biodiesel (Atgur et al., 2022). A significant difference between B_{20} and D_{100} within compression and expansion strokes under a no-load condition was reported. A CFD energy analysis of B_{100} and D_{100} was done on combustion heat transfer, inlet, and exhaust flow properties using MATLAB by Potdukhe and Deshmukh, (2015), while a particulate filter on boundary-layer wall flow with biofuel was reported (Orihuela et al., 2019). Numerical studies have been conducted to investigate the influence of piston-bowl geometrical design (Deresso et al., 2022) on the HRR of engine performance, while others calculate the HRR with experimental validation (Mauro et al., 2018; Dubov et al., 2021). The application of a control system to the blending process of fuel and corrosion

TABLE 1 Physicochemical properties of *Khaya senegalensis* blends.

Property	Sample					ASTM		
	B_5	B_{15}	B_{25}	B_{100}	D_{100}	Method	$B_{6\text{-}20}$ (D 7467)	B_{100} (D 6751)
1. Density @ 15°C (Kg/m^3)	862.2	863.4	864.4	874	852.8	AOAC[a]	-	-
2. Kinematic viscosity @ 40°C (mm^2/s)	4.763	4.655	5.005	5.862	4.635	D 445	1.9–4.1	1.9–6
3. Saponification value (mg KOH/g)	95.44	64.52	80.22	121.74	108.78	AOAC[a]	-	-
4. Iodine value (g iodine/100 g)	27.24	12.01	20.47	62.78	182.11	AOAC[a]	-	-
5. Cetane number	97.36	128.19	109.73	77.01	55.5	D 613	40 min	47 min
6. Cloud point (°C)	0.2	0.4	0.7	8.3	0.2	D 2500	Report	Report
7. Pour point (°C)	< −1.5	< −1.5	< −1.5	2	< −1.5	D 97-96a	-	-
8. Smoke point (°C)	68	70	75	89.3	67	D 93	-	-
9. Flash point (°C)	95	97	98	124	83	D 93	125 min	130 min
10. Calorific value–LHV (MJ/kg)	39.905	39.754	39.603	37.443	35.65	AOAC[a]	-	-

[a]AOAC: Association of Official Analytical Chemists standard method of 1995.

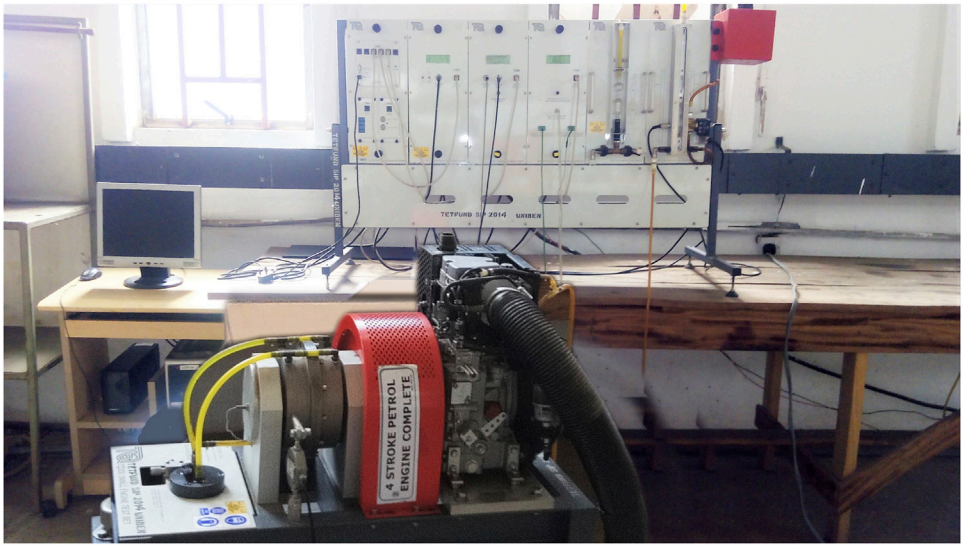

FIGURE 1
Small engine test rig experiment setup.

inhibitor additive blends on a direct injector system was modeled to ensure a stable blending process despite flow velocity perturbation (Mgbemene et al., 2019).

It is necessary to understand how the injected fuel blend characteristics and in-cylinder conditions influence engine combustion outcomes. Hence, this study presents the impact of injector and piston engine elements on the interaction between in-cylinder fluid motion and the combustion chamber environment with respect to the flow effects on engine combustion strength. Attempts to numerically link the effect of fuel blend atomization and mixing strength on the expected performance index were key in this study with experimental validations. The scope of this work majors between compression and power strokes of a single-cylinder CI engine. As was found from the reviewed literature, studies on the fuel flow rate have focused on air and gaseous fuel flows in single- and dual-fuel engines; therefore, this study focused on the liquid fuel flow rate combustion of a homogenous fuel engine.

2 Materials and methods

The physicochemical properties of *Khaya senegalensis* biodiesel blends of 5% of biodiesel to 95% of diesel blend (B_5), 15% of biodiesel to 85% of diesel blend (B_{15}), 25% of biodiesel to 75% of diesel blend (B_{25}), B_{100}, and D_{100} produced experimentally by Onojowho et al. (2019) are given in Table 1. These binary blends are a percentage volumetric proportion of biodiesel and diesel mixed

TABLE 2 Engine specification.

Parameter		Values
1	Dynamometer constant head	1 bar @ 5 L/min (min.)
2	Dynamometer maximum power and speed rating	7.5 KW and 7,000 rpm
3	Engine cylinder/capacity/stroke	Single/0.232 L/4
4	Engine max. rating	3.5 KW @ 3,600 rpm
5	Bore/stroke/crank radius	69/62/31 mm
6	Connecting rod length	104 mm
7	Engine brand/compression ratio	TD212, TQ182785-002/ 22:1
8	Thermocouple	Type-k
9	Gas analyzer model	Testo 330-2LL
10	Injector design	
	Injector type	Multi-hole
	Nozzle tip (hole angle/diameter)	4°/0.22 mm
	Nozzle tip length	2.5 mm
	Nozzle needle valve diameter	4.5 mm
	Hole length	0.6 mm
	Pin height	0.125/0.175 mm
	Sump volume (shell calibration fluid)	0.36 mm
	Pressure	214 ± 4 bar
	Injector brand	Kohler KD 225 series

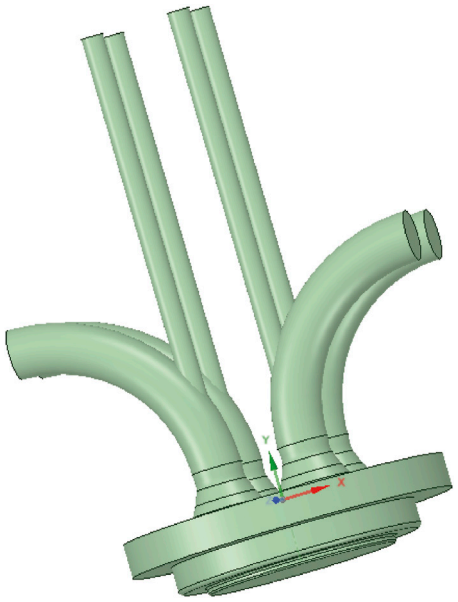

FIGURE 2
Engine 3D model.

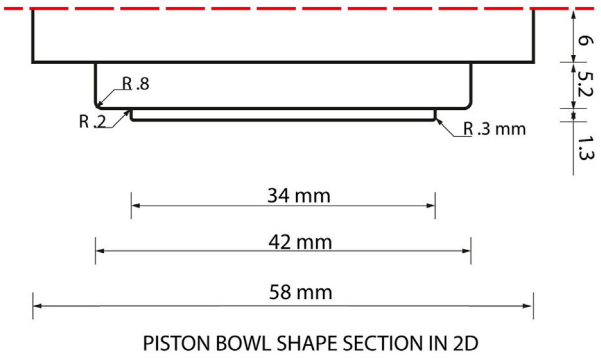

FIGURE 3
Piston bowl shape of the engine model in 2D.

at a stirring speed of 1.5 using the IKA C-MAG HS 4 for 7 min. Before allowing each sample to stand, the TecQuipment Ltd. small engine test rig fitted with a hydraulic dynamometer, as shown in Figure 1 with specifications in Table 2, was applied for the experiment. Each sample was poured into the engine tank, taking turns to flow through the FLOWave SAW flowmeter type 8098. The conical geometry injector fitted into the engine is a multi-hole swirl injection system, design parameters of which are given in Table 2, and generated a swirl on the piston bowl. Combustion efficiency was determined from flue gases using a gas analyzer. By experimentation, the Willans line approach was applied to determine the least piston frictional loss from three selected blends as the FMEP outcome, as shown in Figure 4, at a constant rate of 2,560 rpm. Its low initialization temperature of 300 K was reflected in the combustion temperature. Ansys Fluent v19.R3 software was used to simulate the combustion, and the engine and biodiesel parameters are summarized in Table 3. The HP Z820 Workstation system model was used in this simulation. The engine geometry model was produced on Ansys SpaceClaim having a piston bowl shape and four manifolds, as shown in Figure 2, which was later decomposed to a sector. Figure 3 presents a 2D piston bowl-shaped engine model. The decomposed geometry was meshed into a tri/tetrahedron element-shape type of mesh, and the fine mesh size and total element numbers are shown in Table 3. Deforming the zone mesh sensitivities by applying smoothing and layering mesh methods of the dynamic mesh ensured accuracies. High computational timing was traded-off for accuracy since the total number of elements increases with transition from coarse to fine mesh types. The entire simulation was between the inlet valve closes (IVC) and exhaust valve closing (EVC); however, the compression stroke period of the IVC (225° crank angle [CA] or 45° after bottom dead center [ABDC]) to the fuel valve closes (FVC) (360° CA or 0° before top dead center [BTDC]) of the fuel injection and mixture interaction within the in-cylinder environment is shown in Figure 4. Here, the static temperature is the temperature indicated by the sensor moving concurrently with the mixture velocity. The profile predicted the possible point at which each blend pitches the maximum temperature. A distinct observation was made with each blend with the in-cylinder temperature, indicating that blending viscosity, surface tension, and density together with the velocity, pressure, and temperature

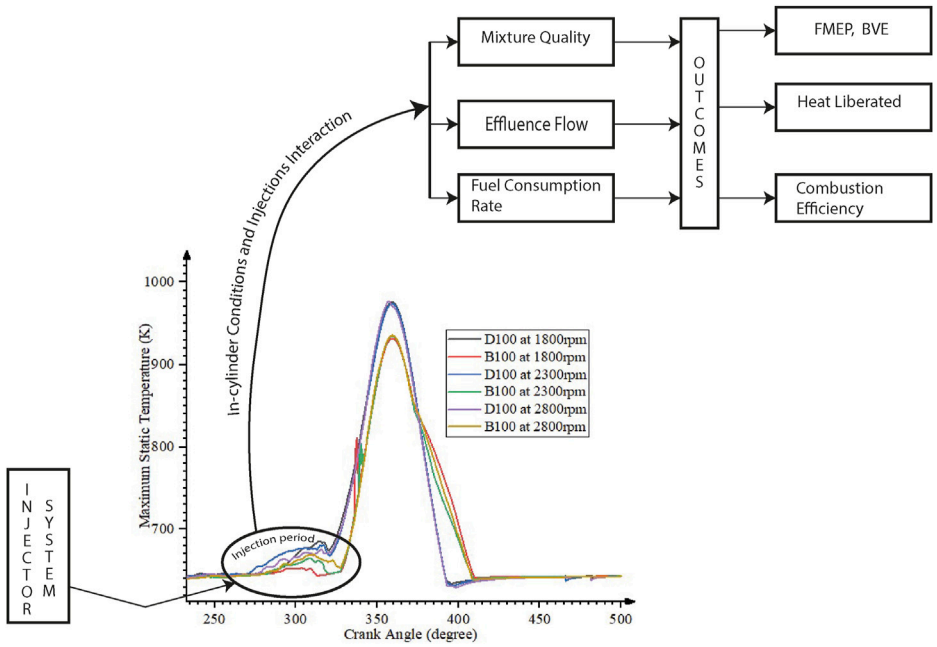

FIGURE 4
Summary of the study focus.

TABLE 3 Combustion simulation parameter summary.

Parameter		Values
1	Inlet valve closes (IVC)	225 *CA* (45° ABDC)
2	Exhaust valve closing (EVC)	500 *CA* (40° BBDC)
3	Compression ratio/equivalence ratio	22:1/0.97
4	Bore/stroke/number of cylinder	69/62 mm/single
5	Engine speed	1,800, 2,300, and 2,800 rpm
6	Injection period (FVO-FVC)	332°–355° *CA*
7	Con rod length and crank radius	104 and 43.28 mm
8	Min./max. valve lift/piston offset	0.2/2 mm/0°
9	Injection spray angle/cetane number	6°/77.01
10	Mesh elements and nodes	123,253 and 162,828
11	Max. and min. mesh size	0.321 and 0.129 mm
12	Thermal conductivity/specific heat	0.14696 W/m^{-k}/2681 J/Kg^{-K}
13	Geometry sector/swirl speed	5°/126, 161, and 196 rpm
14	Injection flow rate/velocity	1.33e-5 (Kg/s)/560 m/s
15	Fuel dynamic viscosity/density	5.12e-3 (Kg/m^{-s})/874 kg/m^3

generates swirl, tumble, and turbulence, significantly contributing to combustion. During the injection period, the profile made by blends suggested the distinct swirl influence of each blend on the engine performance as the engine speed increases. The injection pressure is directly proportional to the engine speed square, and it is a vital response factor in atomization such that the higher the pressure, the better the atomization but not beyond a threshold of creating penetration issues (Taylor, 1985a). In this regard, this simulation considers the injection pressure, angle, velocity, timing, angle, and nozzle diameter to be constant, while the aforementioned blend characteristics with engine speed were varied. The injection diameter at the chamber inlet was 0.00185 m, and the temperature boundary conditions of the walls are as follows: piston, 645 K; valve and chamber, 562 K; and cylinder head, 604 K. Temperature and pressure variable conditions at fluid–wall patched zones were maintained at 404 K and 321,259 Pa, respectively.

2.1 Fundamental models and equations

The renormalized group (RNG) k-ε turbulent kinetic and dissipation energies (Eqs 1, 2) are of the Navier–Stokes viscous model, and the wall treatment from the Menter–Lechner near-wall sub-model was employed in this CFD simulation. The near-wall source term in Eq. 1 accounted for a low Reynolds number effect within the viscous sublayer zone. The dynamic viscosity of B_{100} and D_{100} is 0.00512 and 0.00395 kg/m^{-s}, respectively. The Eddy-Dissipation Concept was considered for the transport species turbulent interaction activities. The maximum swirl target ratio was 1.3, and the swirl speed varied, as presented in Table 3, at increasing engine speed. Although autoignition modeling was applied to the Hardenburg model, accounting for ignition delay per mass fraction of atomized species. The predicted effective fuel flow rate in Eq. 3 hinged on the pressure-swirl atomizer model proposed by Schmidt et al. (1999) built into Ansys Fluent spray models. It describes the centrifugal motion of

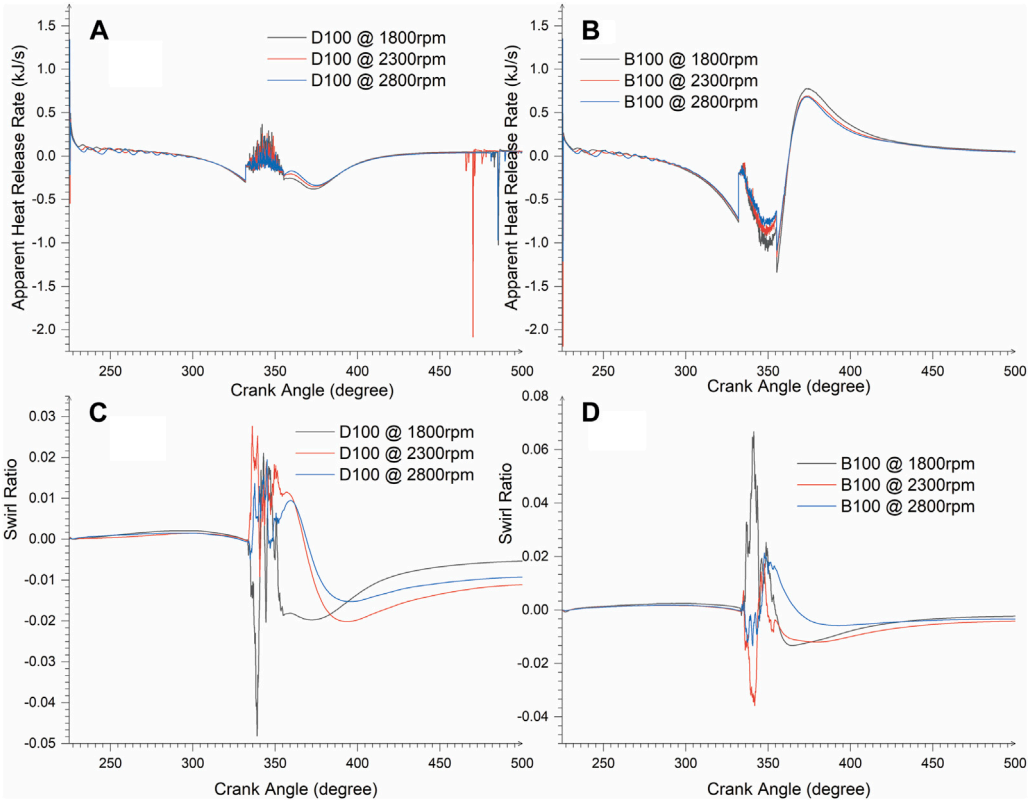

FIGURE 5
CFD predictions of **(A,B)** heat release rate and **(C,D)** swirl ratios for D_{100} and B_{100}.

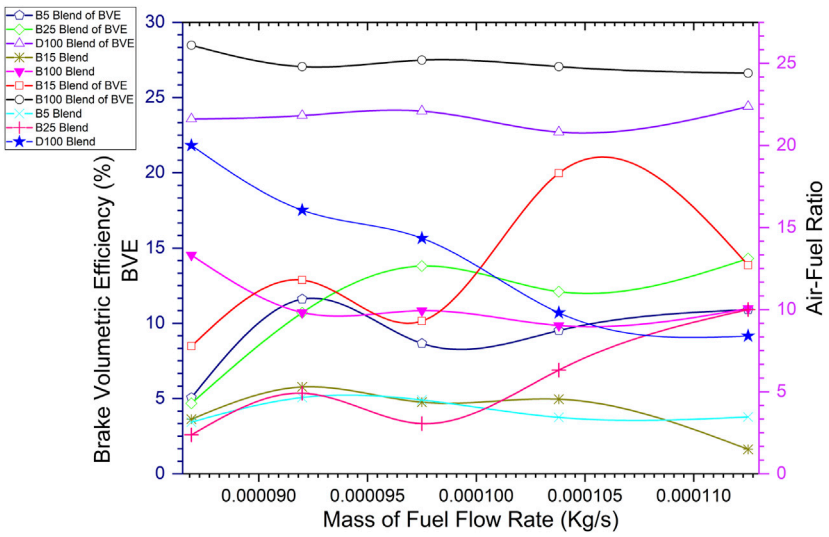

FIGURE 6
Fuel blend flow rate relationship to BVE and air–fuel ratio experiments.

the injected fuel through the inlet port, which forms a film in swirl motion around the valve seat. This forms the bases of primary breakup model film formation through sheet breakup and atomization stages. The atomization model used here depends on the liquid sheet wave growth, while the length of the sheet break up, ligaments, and diameter of ligaments are based on Weber's model in Eq. 6 (Weber, 1931). The Kelvin–Helmholtz–Rayleigh–Taylor (KHRT) spray secondary

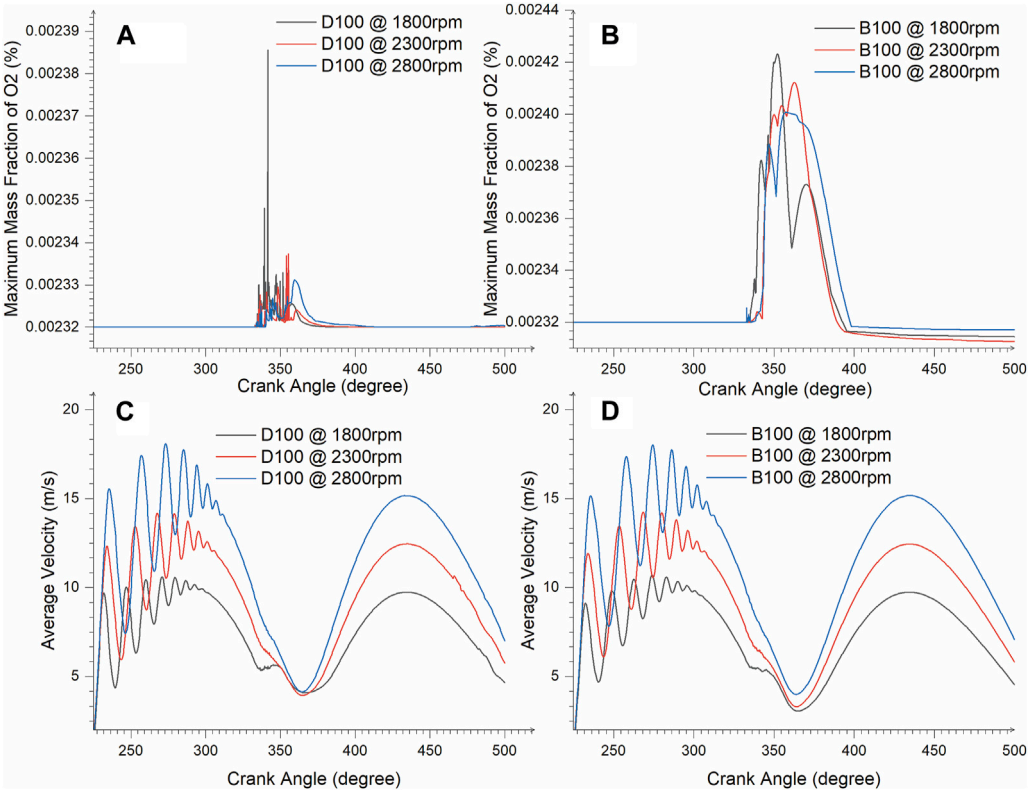

FIGURE 7
In-cylinder effluence flow plots and oxygen consumption at combustion for both blends at varied speeds.

breakup model was chosen due to its high Weber number and high-speed injector system characteristics. The KHRT model is a combination of the Kelvin–Helmholtz wave that forms a liquid core around the injector nozzle with a Levich liquid core breaking length of Eq. 7 and Rayleigh–Taylor injection instabilities on droplet surfaces of Eq. 8. In Ansys Fluent, the non-premixed combustion reaction model is compactable with the diesel ICE because the fuel and oxidizer enter the chamber at different streams. The stoichiometric combustion reaction of fuels satisfies Eq. 9. It should be noted that Eqs 10–16 were applied in the experimentation where fuel and equipment basic data, as used in predictions, were maintained to aid experimental validation. The combustion efficiency (Eq. 15) was embedded into the analyzer, where the condensate heat at the dew point is zeroed for the ICE. Accounting for the accuracies and uncertainties of instruments used in the experimentation, the root square sum approach was applied to determine the overall uncertainty (U_r) (Holman, 2012). Parameter measurements were repeatedly done, and Eq. 17 provides an estimated overall uncertainty.

$$\partial(\rho k)/\partial t + \partial(\rho k u_i)/\partial x_i = \partial\left[\left\{\mu + \left(\rho C_\mu k^2/\varepsilon\right)/\sigma_k\right\}\right]/\partial x_j + G_k - \rho\varepsilon + S_{near-wall}, \quad (1)$$

$$\partial(\rho\varepsilon)/\partial t + \partial(\rho\varepsilon u_i)/\partial x_i = \partial\left[\left\{\mu + \left(\frac{\rho C_\mu k^2}{\varepsilon}\right)/\sigma_\varepsilon\right\}\partial k/\partial x_j\right]/\partial x_j + C_{1\varepsilon}\varepsilon/KG_k - C_{2\varepsilon}\rho\varepsilon^2/K, \quad (2)$$

$$\dot{m}_{eff} = \pi\rho_f u t(d_i - t), \quad (3)$$

$$u = v_c\sqrt{2\Delta P/\rho_f}, \quad (4)$$

$$S_r = \frac{n}{N}, \quad (5)$$

$$d_o = 1.88 d_l(1 + 3\hbar)^{1/6}, \quad (6)$$

$$L = C_l d_o\sqrt{\rho_l/\rho_g}, \quad (7)$$

$$r_c = \pi_{C_{rt}}/k_{rt}, \quad (8)$$

$$C_iH_jO_k + (i + j/4)(O_2 + 3.76N_2) \rightarrow iCO_2 + j/2H_2O + (i + j/4)3.76N_2, \quad (9)$$

$$m_f = \rho_f A_n C_D(\Delta\theta/360N)\sqrt{2\rho_f\Delta P}/1000, \quad (10)$$

$$m_a = C_D(\pi d^2/4)\sqrt{2P_a\Delta P/RT_a}, \quad (11)$$

$$BSFC = 3600 \times 60m_f/2\pi N\tau, \quad (12)$$

$$H_f = m_f \times 10^6 LHV, \quad (13)$$

$$BVE = 60(stroke/2)m_aRT_a/100V_eNP_a \times 100\%, \quad (14)$$

$$\eta_c = 100 - [(T_f - T_a)(A/O_{21} - O_m) + B] - K, \quad (15)$$

$$FMEP = IMEP - BMEP, \quad (16)$$

$$U_r = \left[\sum_{i=1}^{1}\left(u_{x_i}\partial r/\partial x_{i_{x=\bar{x}}}\right)^2\right]^{1/2} = \left[BSFC^2 + BVE^2 + HRR^2 + {\eta_c}^2 + {m_f}^2 + FMEP^2\right]^{1/2} = \pm 5.88. \quad (17)$$

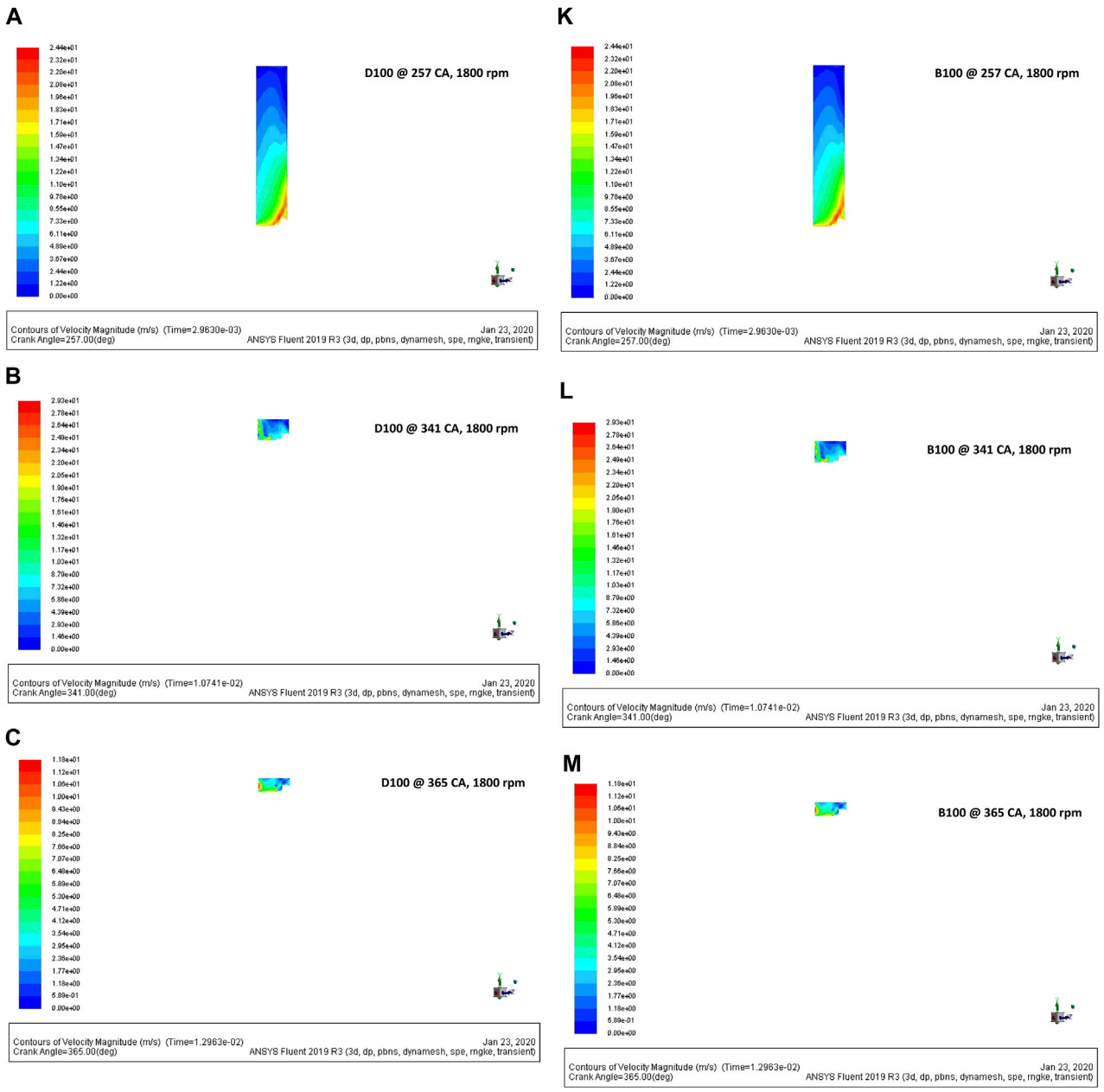

FIGURE 8
(Continued).

3 Results and discussion

3.1 Mixing quality parameter effects

A few mixing quality factors highlighted are in view of revealing their progressive input with respect to the flow rate of *K. senegalensis* biodiesel blends in connection with variation in density, viscosity, and surface tension of fuels on the combustion performance.

3.1.1 Swirling flow attribute

In this direct injection system, the aerodynamics flow nature is promoted by the helical nature of the inlet manifolds and the shape of the valve seat as the external swirl generator and the piston bowl shape as the internal swirl generator. Since strong air motion is desirable irrespective of the injection rate, engine speed variation became a determinant in this simulation. The swirl rapid fluctuation flow period is observed to be so significant during the compression stroke between injection and combustion periods, as shown in Figures 5C, D. The prediction in Figure 5C reveals the buttressing effect of D_{100} higher in-cylinder pressure, irrespective of the engine speed than B_{100}. Keeping a threshold swirl factor of 0.07, D_{100} at 2,300 rpm achieved the highest peak swirl ratio of 0.0272 at 336.15 CA, persisting around that value than the engine speeds of 1,800 and 2,800 rpm, which promoted a longer mixing period. B_{100} at 1,800 rpm achieved the highest peak swirl ratio of

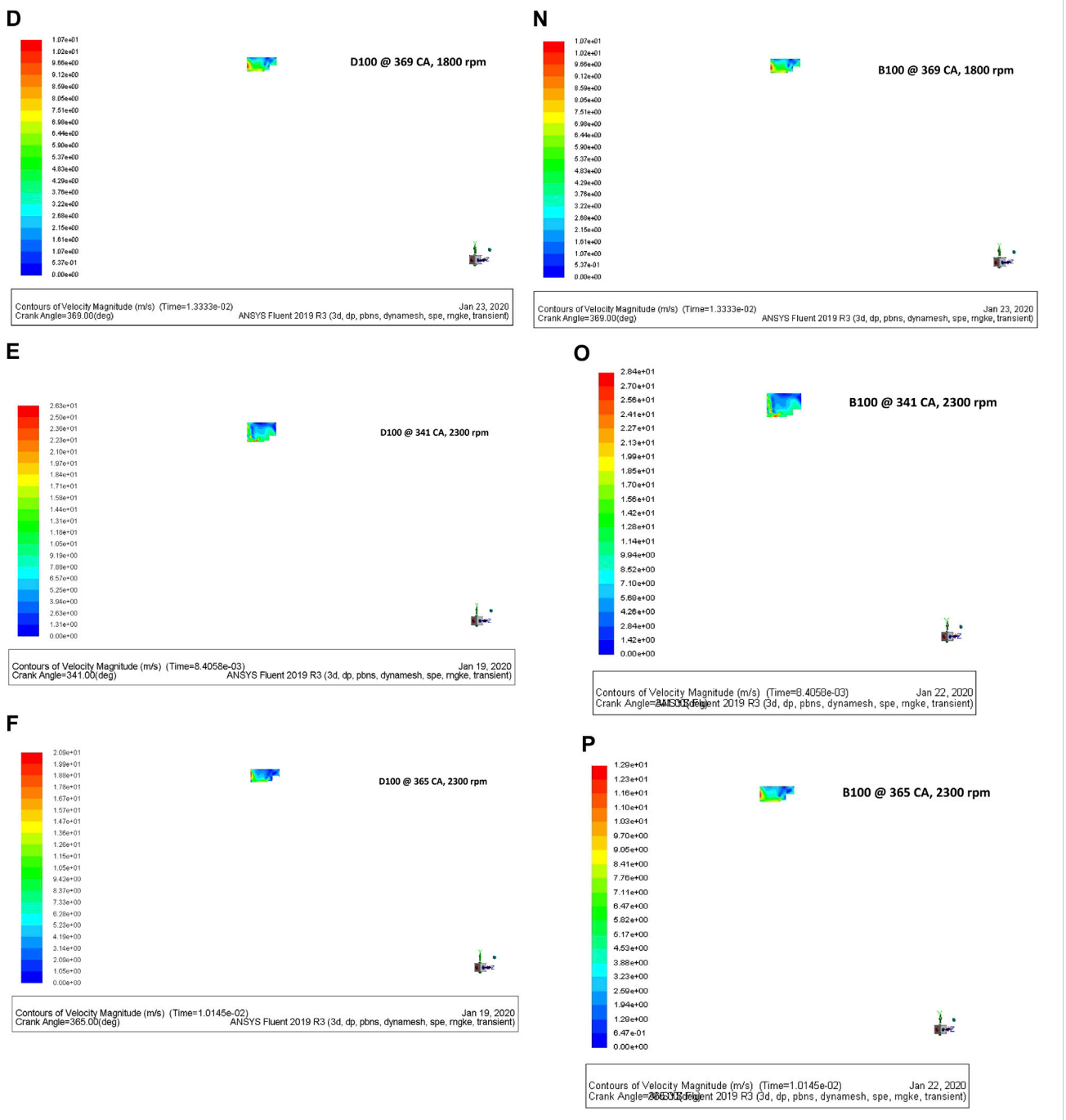

FIGURE 8
(Continued).

0.0668 at 341.3 CA closer to a threshold of 0.07, followed by the performance of 2,800 rpm, as shown in Figure 5D. It can also be observed that 2,300 rpm yielded the least swirl performance, which may affect the mixing length. The notable decrease, similar to that observed by Atgur et al. (2022), observed in both blend swirl ratios is due to the piston movement from the BTDC.

3.1.2 Air–fuel mix effect

The equivalent ratio is ratio of the mass flow rate of air to fuel. The mixture grade is determined by the air–fuel ratio. The CI engine has a grade band of 18–70 (Pulkrabek, 1999); a lower value than this range indicates a very rich mixture, while a value above this range indicates a very lean mixture. However, good combustion could exist around the very rich mixture zone, according to Taylor, (1985a), as shown in Figure 6.

This experiment presents that the air–fuel ratio of all blends reads below 18 even at an increasing flow rate. Increasing the mass fuel flow rate decreases the air–fuel ratio, irrespective of the blends. An implication of this highly rich mixture combustion is that it may result in a decreased in-cylinder

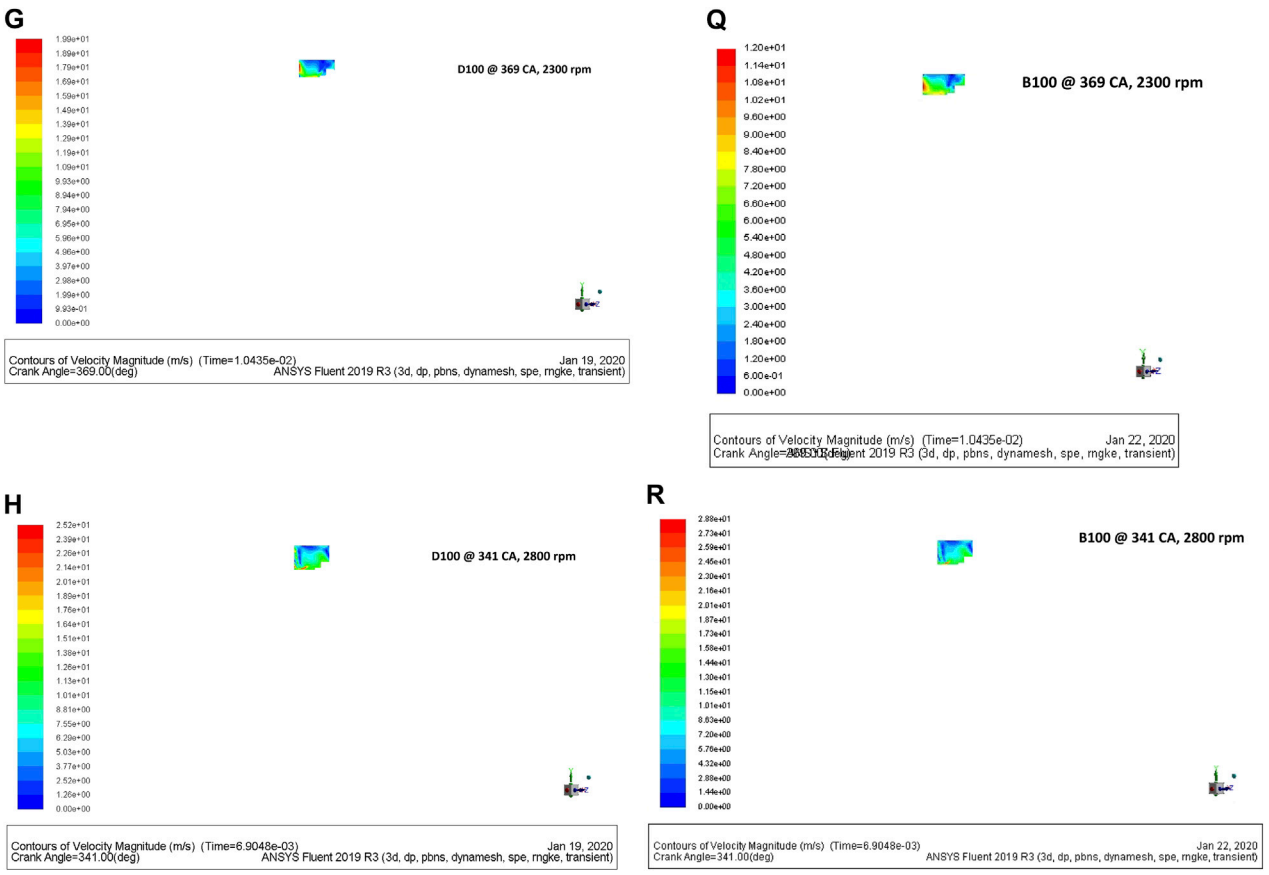

FIGURE 8
(Continued).

combustion pressure and wall temperature and, consequently, increase the ignition delay if the engine depends so much on a high chamber temperature for an ignition. On the other hand, the reduction in the air–fuel ratio reduces the percentage exergy loss during combustion (Van Basshuysen and Schäfer, 2004).

3.1.3 ICE numerical effluence velocity impact of blends

Here, effluence was better studied numerically under the interactive impact of the in-cylinder injection rate, swirl, tumble, squish, and piston motion. As the engine speed increases, the fuel mass injection rate from the single-point nozzle will increase, thus causing turbulence. The piston harmonic motion on the mixture also increases the turbulence result of the above interactions. In Figure 7, the maximum mass fraction of percentage O_2 consumption decreases as speed increases for D_{100} and B_{100}, upholding the decrease response in the air–fuel ratio to the fuel flow rate. However, the higher consumption rate of B_{100} in (b), which negates the experimented expectation of Figure 6, resulted from the O_2 content in B_{100}, whereas D_{100} has a void.

Instantaneous average velocity during compression and expansion strokes is shown in Figures 7C, D. The engine speed positively increased the effluence flow. The injection flow is significant at a speed of 1,800 rpm and negligible at 2,800 rpm due to the increase in turbulence for D_{100} and B_{100}. The turbulence is significantly rapid between 225° CA and 290° CA as the piston moves from the BDC to TDC. This rapid flow increases with increase in the engine speed, especially around the wall, as presented in the contours. Immediately after the compression stroke, the minimum effluence existed for both blends at all varied speed. The least is 3.05414 m/s at 365° CA, and the highest is 3.99833 m/s at 364° CA for B_{100} of 1,800 and 2,800 rpm, respectively, while the least is 3.93886 m/s at 365° CA and the highest is 4.14176 m/s at 364.75° CA for B_{100} at 2,300 and 2,800 rpm, respectively. The contours shown in Figure 8 provides clearer visualization. Piston upward motion from the BTDC creates higher turbulence at the wall from the tumble and squish of fluid in (a) and (k). During the injection period, the swirl produced from the nozzle through the piston surface is higher. The interaction of fuel density, viscosity, and surface tension plays out here. At 2,300 and 2,800 rpm, B_{100} creates higher mixing characteristics due to its higher fuel physical properties. This proper mixing, together with higher cetane number and lower heating value (LHV) of B_{100}, promoted a longer combustion period than D_{100}, as shown in Figure 4. During combustion, the effluence severity appears to be greater for both fuels, massive on the wall and piston surface. Immediately after the compression stroke at 369° CA, B_{100} seemed to possess higher turbulence, which could have stemmed from prolonged combustion.

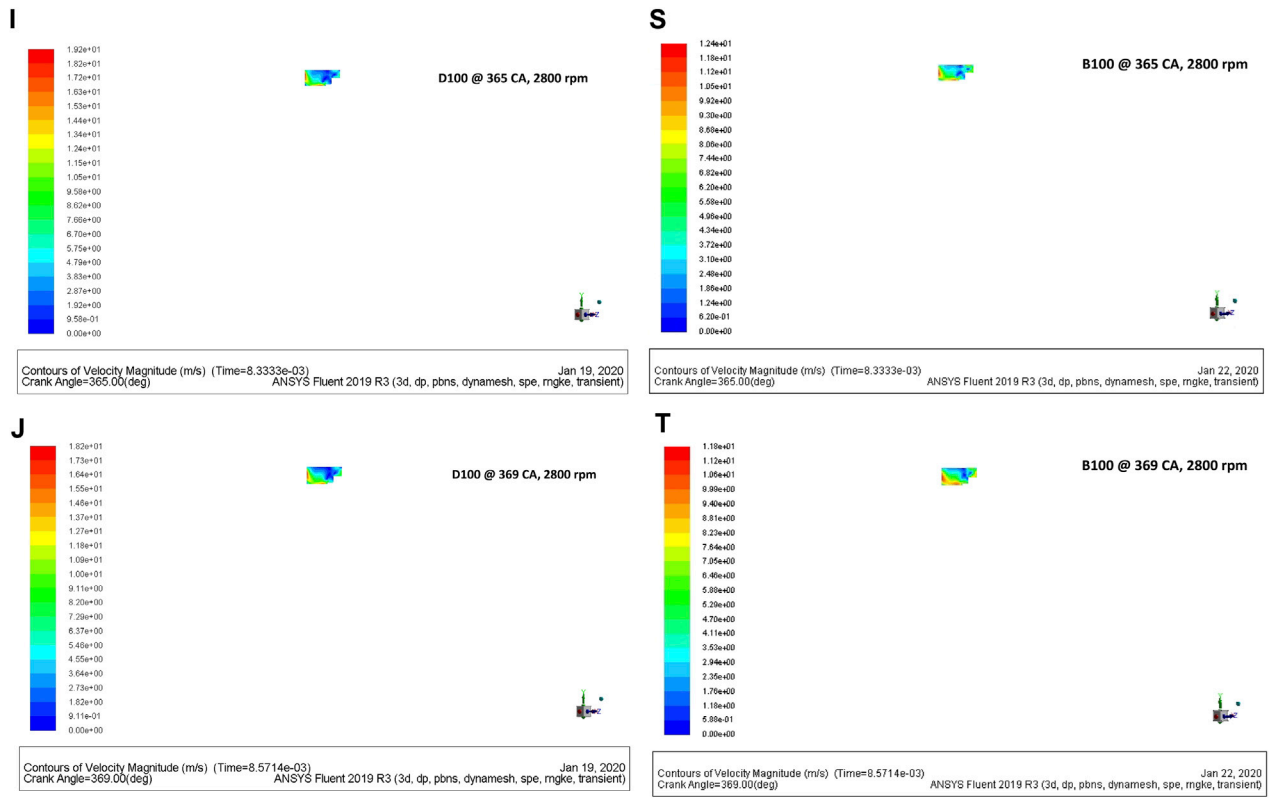

FIGURE 8
(Continued). Velocity contour depicting in-cylinder effluence. Injection period: **(B,E,H,L,O,R).** During combustion period: **(C,F,I,M,P,S).** After compression stroke: **(D,G,J,N,Q,T)**. **(A–T)** are comparison of B100 and D100 blends at specific CA and speeds respectively).

3.2 Blends effect on fuel consumption

Increasing the load or torque on the engine causes a higher fuel mass flow rate. Applying the fuel flow rate to the BSFC relationship on the blending effect, as shown in Figure 9, presents that the blending increase in pure biodiesel causes a reduction effect on fuel consumption as the fuel flow rate increases. B_5 relatively made the highest consumption rate. Ambarita (2018) obtained a similar trend with this study. BSFC is a derived parameter like others in Table 4. Hence, their range and accuracy were not specified on the instrument. All uncertainties were within their 95% level of acceptance. This indicates that errors were quite small for each parameter and even the overall system.

3.3 Engine performance expectation

3.3.1 Mixture efficiency: BVE

It is expected that the BVE positively responds to the increasing air mass flow rate and inversely to engine speed. This provides a brief idea of the engine breathing capacity in the combustion process. Figure 6 shows blend mixing performance on the fuel flow rate relation from the experiment. The BVE of blends increases as the flow rate increases, where B_5 yielded the lowest response even at 0.0001125 kg/s, thus yielding 10.9% efficiency. Relatively, the highest performing blend is B_{100} with 24.8% efficiency, followed by D_{100} with 22.7% efficiency, specifically at 0.0001038 kg/s.

3.3.2 Combustion efficiency outcome

On a holistic performance, all fuel blends were well-burned. The engine is well capable of combusting at a higher fuel flow rate as the burning efficiency increases. The combustion trend is in coherence with the BVE of fuel mixtures, projecting combustion efficiencies to respond positively to the increasing blending proportion of biodiesel, as shown in Figure 10. The increasing trend of blend efficiency is similar to that studied by Li et al. (2022). The least burned fuel blend was B_5 with 54.5%, while B_{100} had 81.47%, and D_{100} had 88.06% at 0.0001125 kg/s or 75% loading capacity.

3.3.3 Engine heat liberation rate outcome

Figures 5A, B show the engine modeling of the HRR for D_{100} and B_{100} respectively. It was a zero-heat loss-based assumption; hence, it is called the apparent HRR. Heat transfer from the mixture to the chamber was indicated by the negative decrease from zero. Rapid combustion was predicted to start at 335° CA for both blends, irrespective of the engine speed to approximately 380° CA for D_{100} and 430° CA for B_{100}. The HRR was predicted to occur in two phases. The first phase was at the spontaneous ignition period, as shown in Figure 4. The second phase was characterized with a significant swirl-amplified ripple occurring at the heart of the combustion

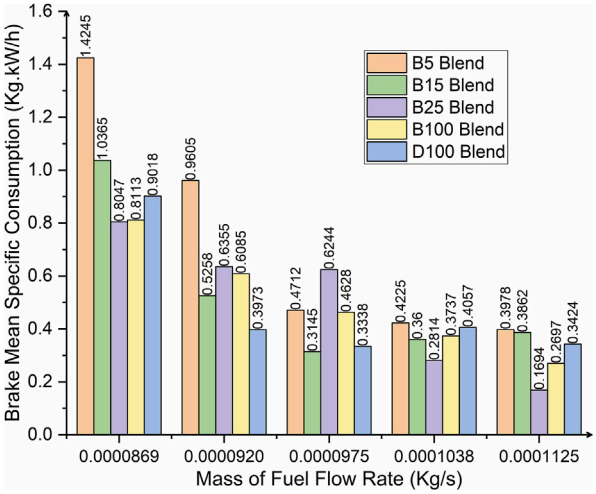

FIGURE 9
Fuel flow rate and blending effect on engine consumption.

TABLE 4 Accuracies and uncertainty of measurements.

Parameter		Range	Accuracy	Uncertainty
1	BSFC	-	-	±0.2 kg kW/h
2	BVE	-	-	±0.62%
3	HRR	-	-	±5.55 W
4	η_c	0%–120%	±0.6%	±1.83%
5	m_f	0–260,000 kg/h	±0.5%	±9.55 × 10^{-6} kg/s
6	FMEP	-	-	±0.11 bar

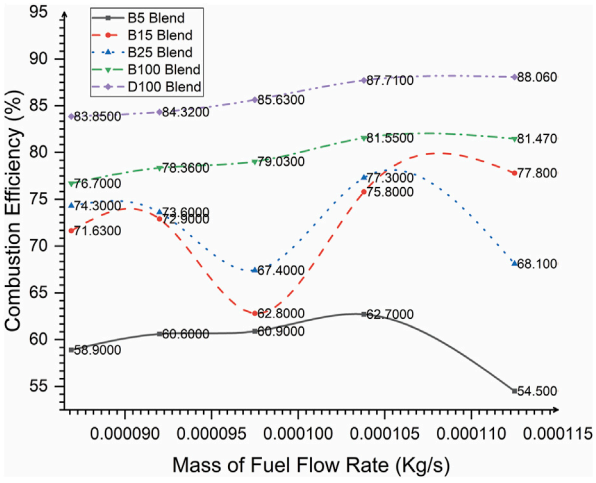

FIGURE 10
Fuel blend effect on combustion efficiency.

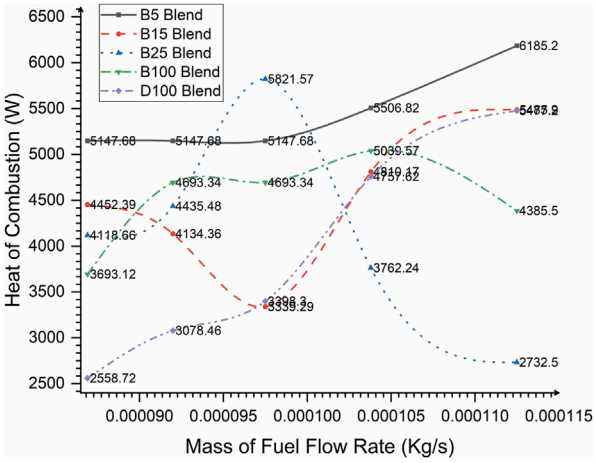

FIGURE 11
Engine heat liberation rate.

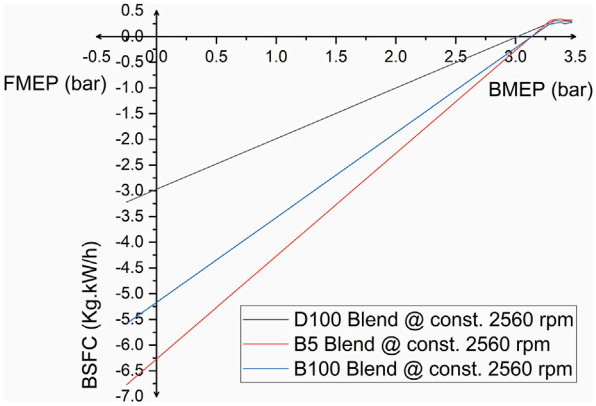

FIGURE 12
Piston frictional losses.

period. The highest peak of the HRR D_{100} was predicted as 0.36892 kJ/s at 342.1° CA, 0.26226 kJ/s at 342.3° CA, and 0.2261 kJ/s at 343.05° CA for 1,800 rpm, 2,300 rpm, and 2,800 rpm, respectively. These peaks occurred at about the ignition period, and the profile of D_{100} is an inverse of that of B_{100} at all speeds. This explains the lower activation energy requirement of B_{100}; hence, the higher compression temperature and pressure of D_{100} yielded a rapid ignition rate, as obtained by Atgur et al. (2022). However, B_{100} achieved the highest peaks of the HRR with 0.78063 kJ/s at 373.25° CA, 0.69362 kJ/s at 373° CA, and 0.6811 kJ/s at 373° CA prior to combustion decay for a speed of 1,800 rpm, 2,300 rpm, and 2,800 rpm, respectively. This HRR profile may have also been influenced by the piston bowl-shaped design, as obtained by Deresso et al. (2022). The influence of the engine speed on the HRR in D_{100} states and an increase in speed provided an increase in heat release, whereas B_{100} obtained an opposite effect. From experimental validation, the fuel flow rate and heating value are directly proportional to the heat of combustion, as shown in Figure 11. Heat liberated from B_{100} is higher than that in D_{100}; however, a steady increase was observed with D_{100} as against B_{100} with respect to the flow rate pointing to the aforementioned speed effect. The blend with the best yield was B_5 as it yields the highest

heat liberation under an increasing fuel flow rate, as specified on the profile.

3.3.4 Fuel blends and engine losses

During the compression of a mixture, the piston loses some useful energy in overcoming friction. As shown in Figure 12, D_{100} lost useful pressure force of 3 bar to in-cylinder friction, while B_{100} and B_5 lost 3.136 bar and 3.135 bar, respectively, at constant speed. This suggests that diesel possesses a more lubricating effect and would offer a better exergy advantage than B_5 and B_{100} blends.

4 Conclusion

This study successfully presented a numerical and experimentally validated behavior of the fuel blend flow rate on the ICE, showcasing specific observations on combustion. In other words, the fuel mass flow rate generated by an injector and piston motion significantly affected the engine combustion strength.

- ➢ Fuel–air mixing quality impacts the ICE combustion performance indexing. Fuel consumption reduces when the biodiesel blending ratio and mass flow rate increase.
- ➢ Engine breathing efficiency increases at a higher fuel mass flow rate, causing a high burning efficiency of blends. This is the engine stability response to the loading effect.
- ➢ Engine combustion efficiency could be effectively determined *via* flue gas up to an 88% accuracy level as the fuel mass flow rate increases.
- ➢ An ignition delay period of 3° CA CFD prediction will be common to diesel and biodiesel, irrespective of the speed effect; however, biodiesel will have a longer combustion duration.
- ➢ The fuel mass flow rate increase increases the heat of fuel combustion experimentally. The engine speed effect on the heat liberation rate causes a contrary behavior on biodiesel and diesel fuels when compared numerically.
- ➢ Lastly, D_{100} offers lower frictional loss than B_{100} and B_5 in an engine. By the FMEP approach, D_{100} projects better lubricating and exergy advantages.

Data availability statement

The original contributions presented in the study are included in the article/Supplementary Material; further inquiries can be directed to the corresponding author.

Author contributions

EO: funding acquisition, investigation, and writing–original draft. AA: supervision and writing–review and editing.

Funding

The author(s) declare that financial support was received for the research, authorship, and/or publication of this article. This research was self-funded.

Acknowledgments

The authors thank the staff and management of the Mechanical Engineering Department, University of Benin, for granting access to their laboratory and equipment.

Conflict of interest

The authors declare that the research was conducted in the absence of any commercial or financial relationships that could be construed as a potential conflict of interest.

Publisher's note

References

Abdullah, N. R., Zaharin, M. S. M., Mamat, A. M. I., Nawi, M. R. M., and Sharudin, H. (2015). Effects of ethanol blends on gasoline engine performance and exhaust emissions. *J. Teknol.* 76. doi:10.11113/jt.v76.5920

Akar, M. A. (2016). Performance and emission characteristics of compression ignition engine operating with false flax biodiesel and butanol blends. *Adv. Mech. Eng.* 2, 168781401663267–7. doi:10.1177/1687814016632677

Al-Hasan, M. I., and Al-Momany, M. (2008). The effect of iso-butanol-diesel blends on engine performance. *Transport* 23, 306–310. doi:10.3846/1648-4142.2008.23.306-310

Ambarita, H. (2018). Effect of engine load and biogas flow rate to the performance of a compression ignition engine run in dual-fuel (dieselbiogas) mode. *IOP Conf. Ser. Mater. Sci. Eng.* 309, 012006. doi:10.1088/1757-899X/309/1/012006

Atelge, M. R., Arslan, E., Krisa, D., Al-Samaraae, R. R., Abut, S., Ünalan, S., et al. (2022). Comparative investigation of multi-walled carbon nanotube modifed diesel fuel and biogas in dual fuel mode on combustion, performance, and emission characteristics. *Fuel* 313, 1–15. doi:10.1016/j.fuel.2021.123008

Atgur, V., Manavendra, G., Pandurangarao Desai, G., and Nageswara Rao, B. (2022). "CFD combustion simulations and experiments on the blended biodiesel two-phase engine flows," in *Computational fluid dynamics [working title] (IntechOpen)*. doi:10.5772/intechopen.102088

Caligiuri, C., Bietresato, M., and Renzi, M. (2019). The effect of using diesel-biodiesel-bioethanol blends on the fuel feed pump of a small-scale internal combustion engine. *Energy Procedia* 158, 953–958. doi:10.1016/j.egypro.2019.01.235

Chen, Z., Zuo, W., Zhou, K., Li, Q., Huang, Y., and E, J. (2023). Multi-objective optimization of proton exchange membrane fuel cells by RSM and NSGA-II. *Energy Convers. Manag.* 277, 116691. doi:10.1016/j.enconman.2023.116691

Daud, S., Hamidi, M. A., and Mamat, R. (2022). A review of fuel additives' effects and predictions on internal combustion engine performance and emissions. *AIMSE* 10, 1–22. doi:10.3934/energy.2022001

Deng, B., Li, Q., Chen, Y., Li, M., Liu, A., Ran, J., et al. (2018). The effect of air/fuel ratio on the CO and NOx emissions for a twinspark motorcycle gasoline engine under

wide range of operating conditions. *Energy* 169, 1202–1213. doi:10.1016/j.energy.2018.12.113

Deresso, H., Nallamothu, R. B., Ancha, V. R., and Yoseph, B. (2022). Numerical study of different shape design of piston bowl for diesel engine combustion in a light duty single-cylinder engine. *Heliyon* 8, e09602–e09610. doi:10.1016/j.heliyon.2022.e09602

Dubov, G., Bogomolov, A., Azikhanov, S., Strelnikov, P., and Nokhrin, S. (2021). Temperature parameters in the combustion chambers of CUMMINS KTA-50 engines operating on various fuels under different fuel consumption rates. *E3S Web Conf.* 315, 03011. doi:10.1051/e3sconf/202131503011

Estrada, L., Moreno, E., Gonzalez-Quiroga, A., Bula, A., and Duarte-Forero, J. (2022). Experimental assessment of performance and emissions for hydrogen-diesel dual fuel operation in a low displacement compression ignition engine. *Heliyon* 8, 092855–e9311. doi:10.1016/j.heliyon.2022.e09285

Feng, R., Chen, K., Sun, Z., Hu, X., Li, G., Wang, S., et al. (2022). A comparative study on the energy flow of a hybrid heavy truck between AMT and MT shift mode under local driving test cycle. *Energy Convers. Manag.* 256, 115359–115416. doi:10.1016/j.enconman.2022.115359

Feng, R., Li, G., Sun, Z., Hu, X., Deng, B., and Fu, J. (2023). Potential of emission reduction of a turbo-charged non-road diesel engine without aftertreatment under multiple operating scenarios. *Energy* 263, 125832–125915. doi:10.1016/j.energy.2022.125832

Feroskhan, M., Ismail, S., Kumar, A., Kumar, V., and Aftab, S. K. (2017). Investigation of the effects of biogas flow rate and cerium oxide addition on the performance of a dual fuel CI engine. *Biofuels* 8, 197–205. doi:10.1080/17597269.2016.1215072

Gnanamoorthi, V., and Vimalananth, V. T. (2020). Effect of hydrogen fuel at higher flow rate under dual fuel mode in CRDI diesel engine. *Int. J. Hydrogen Energy* 45, 16874–16889. doi:10.1016/j.ijhydene.2020.04.145

Holman, J. P. (2012). *Experimental methods for engineers*. 8th ed. Boston: McGraw-Hill/Connect Learn Succeed.

Jamrozik, A., Tutak, W., and Grab-Rogaliński, K. (2022). Effects of propanol on the performance and emissions of a dual-fuel industrial diesel engine. *Appl. Sci.* 12, 5674. doi:10.3390/app12115674

Karami, R., Rasul, M. G., Khan, M. M. K., and Anwar, M. (2019). Performance analysis of direct injection diesel engine fueled with diesel-tomato seed oil biodiesel blending by ANOVA and ANN. *Energies* 12, 4421. doi:10.3390/en12234421

Knauder, C., Allmaier, H., Sander, D. E., and Sams, T. (2019). Investigations of the friction losses of different engine concepts. Part 1: a combined approach for applying subassembly-resolved friction loss analysis on a modern passenger-car diesel engine. *Lubricants* 7, 39. doi:10.3390/lubricants7050039

Küçükosman, R., Yontar, A. A., and Ocakoglu, K. (2022). Nanoparticle additive fuels: atomization, combustion and fuel characteristics. *J. Anal. Appl. Pyrolysis* 165, 105575. doi:10.1016/j.jaap.2022.105575

Kumar, P., and Rehman, A. (2014). Performance and emission characteristics of dual injection in compression ignition (CI) engine. *Int. J. Automob. Eng. Res. Dev.* 4, 15–28.

Li, Z., Wang, Z., Mo, H., and Wu, H. (2022). Effect of the air flow on the combustion process and preheating effect of the intake manifold burner. *Energies* 15, 3260. doi:10.3390/en15093260

Liu, H., Wang, Z., Wang, J., He, X., Zheng, Y., Tang, Q., et al. (2015a). Performance, combustion and emission characteristics of a diesel engine fueled with polyoxymethylene dimethyl ethers (PODE3-4)/diesel blends. *Energy* 88, 793–800. doi:10.1016/j.energy.2015.05.088

Liu, J., Yao, A., and Yao, C. (2015b). Effects of diesel injection pressure on the performance and emissions of a HD common-rail diesel engine fueled with diesel/methanol dual fuel. *Fuel* 140, 192–200. doi:10.1016/j.fuel.2014.09.109

Mahla, S. K., Das, L. M., and Gupta, N. (2017). Effects of CNG flow rate on combustion, performance and emissions characteristics of biodiesel fuelled diesel engine. *Int. J. ChemTech Res.* 10, 228–240.

Mao, G., Shi, K., Zhang, C., Chen, S., and Wang, P. (2020). Experimental research on effects of biodiesel fuel combustion flame temperature on NOX formation based on endoscope high-speed photography. *J. Energy Insti.* 93, 1399–1410. doi:10.1016/j.joei.2020.01.002

Mauro, S., Şener, R., Gül, M. Z., Lanzafame, R., Messina, M., and Brusca, S. (2018). Internal combustion engine heat release calculation using single-zone and CFD 3D numerical models. *Int. J. Energy Environ. Eng.* 9, 215–226. doi:10.1007/s40095-018-0265-9

Mgbemene, C. A., Kalu-Uka, A. C., Odukwe, A. O., Kalu-Uka, G. M., Ezema, I. C., and Ogbuka, C. U. (2019). Analysis of an automatic control system for the blending of petrol with corrosion inhibitor in cranked. Direct continuous electronic fuel injection (DC-EFI) automobile engines. *Int. J. Eng. Res.* 6 doi:10.17577/IJERTV8IS060338

Mishra, P. C. (2013). Modeling for friction of four stroke four cylinder in-line petrol engine. *Tribol. Ind.* 35, 237–245.

Mohammed, M. K., Balla, H. H., Al-Dulaimi, Z. M. H., Kareem, Z. S., and Al-Zuhairy, M. S. (2021). Effect of ethanol-gasoline blends on SI engine performance and emissions. *Case Stud. Therm. Eng.* 25, 100891. doi:10.1016/j.csite.2021.100891

Onojowho, E. E., Obayopo, S. O., and Asere, A. A. (2019). "Optimization of biodiesel production from Khaya senegalensis oil using heterogeneous catalyst," in *Diversification of developing economies: imperatives for sustainable environment and technological innovations* (Ile-Ife: African Centre of Excellence, Obafemi Awolowo University, Ile-Ife.: OAU Printing Press), 388. Available at: www.oautekconf.org.

Onukwuli, O. D., Esonye, C., and Ofoefule, A. U. (2021). Combustion exhaust release impact, diesel engine performance, and optimization studies of green diesel-petrodiesel blend in a high compression ratio direct-injection compression-ignition engine. *Adv. Mech. Eng.* 13, 168781402110187. doi:10.1177/16878140211018778

Orihuela, M. P., Haralampous, O., Chacartegui, R., Torres García, M., and Martínez-Fernández, J. (2019). Numerical simulation of a wall-flow particulate filter made of biomorphic silicon carbide able to fit different fuel/biofuel inputs. *Processes* 7, 945. doi:10.3390/pr7120945

Park, H., Shim, E., Lee, J., Oh, S., Kim, C., Lee, Y., et al. (2022). Large–squish piston geometry and early pilot injection for high efficiency and low methane emission in natural gas–diesel dual fuel engine at high–load operations. *Fuel* 308, 122015. doi:10.1016/j.fuel.2021.122015

Parthasarathy, M., Ramkumar, S., and Isaac Joshua Ramesh Lalvani, J. (2019). Influence of various flow rates of CNG in CI engine with blend of tamanu methyl ether and ethanol. *Int. J. Veh. Struct. Syst.* 11. doi:10.4273/ijvss.11.2.06

Perumal Venkatesan, E., Balasubramanian, D., Samuel, O. D., Kaisan, M. U., and Murugesan, P. (2021). "Effect of hybrid nanoparticle on DI diesel engine performance, combustion, and emission studies," in *Novel internal combustion engine technologies for performance improvement and emission reduction energy, environment, and sustainability*. Editors A. P. Singh and A. K. Agarwal (Singapore: Springer Singapore), 235–263. doi:10.1007/978-981-16-1582-5_10

Pham, Q., Park, S., Agarwal, A. K., and Park, S. (2022). Review of dual-fuel combustion in the compression-ignition engine: spray, combustion, and emission. *Energy* 250, 123778. doi:10.1016/j.energy.2022.123778

Potdukhe, S. P., and Deshmukh, M. M. (2015). Modeling and energy analysis of a diesel and biodiesel fuelled engine. *Int. J. Sci. Res.* 4, 89–93.

Prasad, K. S., and Saravanan, R. (2021). Study of impact of CNG flow rate and speed on the performance and emission characteristics of DTSI engine using petrol-ethanol fuel blend. *J. Mech. Eng. Res. Dev.* 44, 01–09.

Pulkrabek, W. W. (1999). *Engineering fundamentals of the internal combustion engine*. First edition. Upper Saddle River, New Jersey 07458: Prentice Hall.

Rai, A., Kumar, D., Sonawane, U., and Agarwal, A. K. (2021). "Dimethyl ether spray characteristics for compression ignition engines," in *Novel internal combustion engine technologies for performance improvement and emission reduction energy, environment, and sustainability*. Editors A. P. Singh and A. K. Agarwal (Singapore: Springer Singapore), 79–103. doi:10.1007/978-981-16-1582-5_4

Said, Z., Le, D. T. N., Sharma, P., Dang, V. H., Le, H. S., Nguyen, D. T., et al. (2022). Optimization of combustion, performance, and emission characteristics of a dual-fuel diesel engine powered with microalgae-based biodiesel/diesel blends and oxyhydrogen. *Fuel* 326, 124987. doi:10.1016/j.fuel.2022.124987

Schmidt, D. P., Nouar, I., Senecal, P. K., Rutland, C. J., Martin, J. K., and Reitz, R. D. (1999). *Pressure-swirl atomization in the near field*. Warrendale, Pa, USA: SAE.

Shaafi, T., and Velraj, R. (2015). Influence of alumina nanoparticles, ethanol and isopropanol blend as additive with diesel-soybean biodiesel blend fuel: combustion, engine performance and emissions. *Renew. Energy* 80, 655–663. doi:10.1016/j.renene.2015.02.042

Shahabuddin, M., Liaquat, A. M., Masjuki, H. H., Kalam, M. A., and Mofijur, M. (2013). Ignition delay, combustion and emission characteristics of diesel engine fueled with biodiesel. *Renew. Sustain. Energy Rev.* 21, 623–632. doi:10.1016/j.rser.2013.01.019

Stępień, Z., Pielecha, I., Szwajca, F., and Cieślik, W. (2022). Effects of ethanol admixtures with gasoline on fuel atomization characteristics using high-pressure injectors. *Energies* 15, 2926. doi:10.3390/en15082926

Sun, D., Cai, W., Li, C., and Lu, J. (2021). Experimental study on atomization characteristics of high-energy-density fuels using a fuel slinger. *Energy* 234, 121222. doi:10.1016/j.energy.2021.121222

Taylor, C. F. (1985a). *The internal-combustion engine in theory and practice. Volume 11: combustion, fuels, materials, design*. 2nd ed. Cambridge, Mass: M.I.T. Press. rev.

Taylor, C. F. (1985b). *The internal-combustion engine in theory and practice. Volume I: thermodynamics, fluid flow, performance*. 2nd ed. Cambridge, Mass: M.I.T. Press. rev.

Ude, C. N., Onukwuli, O. D., Nwobi –Okoye, C., Anisiji, O. E., Atuanya, C. U., and Menkiti, M. C. (2020). Performance evaluation of cottonseed oil methyl esters produced using CaO and prediction with an artificial neural network. *Biofuels* 11, 77–84. doi:10.1080/17597269.2017.1345355

Van Basshuysen, R., and Schäfer, F. (2004). *Internal combustion engine handbook: basics, components, systems, and perspectives* (Warrendale, Pa: SAE International).

Weber, C. (1931). Zum Zerfall eines Flüssigkeitsstrahles. *ZAMM* 11, 136–154. doi:10.1002/zamm.19310110207

Wysocki, O., Kropiwnicki, J., Zajdziński, T., and Czyżewicz, J. (2018). Experimental determination of general characteristic of internal combustion engine using mobile test bench connected via Power Take-Off unit. *IOP Conf. Ser. Mater. Sci. Eng.* 421, 042087. doi:10.1088/1757-899X/421/4/042087

Yamin, J. A., and Hdaib, I. I. (2022). Analysis of internal combustion engine performance using design of experiment. *Teh. Vjesn.* 29. doi:10.17559/TV-20210312194600

Zardoya, A. R., Lucena, I. L., Bengoetxea, I. O., and Orosa, J. A. (2022). Research on an internal combustion engine with an injected pre-chamber to operate with low methane number fuels for future gas flaring reduction. *Energy* 253, 124096. doi:10.1016/j.energy.2022.124096

Zuo, W., Chen, Z., E, J., Li, Q., Zhang, G., and Huang, Y. (2023a). Effects of structure parameters of tube outlet on the performance of a hydrogen-fueled micro planar combustor for thermophotovoltaic applications. *Energy* 266, 126434. doi:10.1016/j.energy.2022.126434

Zuo, W., Li, D., E, J., Xia, Y., Li, Q., Quan, Y., et al. (2023b). Parametric study of cavity on the performance of a hydrogen-fueled micro planar combustor for thermophotovoltaic applications. *Energy* 263, 126028. doi:10.1016/j.energy.2022.126028

Zuo, W., Wang, Z., E, J., Li, Q., Cheng, Q., Wu, Y., et al. (2023c). Numerical investigations on the performance of a hydrogen-fueled micro planar combustor with tube outlet for thermophotovoltaic applications. *Energy* 263, 125957. doi:10.1016/j.energy.2022.125957

Zuo, W., Zhang, Y., E, J., Li, J., Li, Q., and Zhang, G. (2022). Performance comparison between single S-channel and double S-channel cold plate for thermal management of a prismatic LiFePO4 battery. *Renew. Energy* 192, 46–57. doi:10.1016/j.renene.2022.04.116

Nomenclature

IVC	Inlet valve closes
EVC	Exhaust valve closes
FVC	Fuel valve closes
FVO	Fuel valve opens
ABDC	After bottom dead center
BBDC	Before bottom dead center
BTDC	Before top dead center
HCCI	Homogeneous charge compression ignition
CFD	Computational fluid dynamics
CNG	Compressed natural gas
RNG	Renormalized group
CMEP	Charging mean effective pressure
AI	Artificial intelligence
FMEP	Frictional mean effective pressure
IMEP	Indicated mean effective pressure
AMEP	Auxiliary-driving mean effective pressure
ICE	Internal combustion engine
PMEP	Power-gaining mean effective pressure
SI	Spark ignition
MMEP	Mechanical mean effective pressure
CI	Compression ignition
BMEP	Brake mean effective pressure
CA	Crank angle
TMEP	Turbine-added mean effective pressure
BVE	Brake volumetric efficiency
BSFC	Brake-specific fuel consumption
LHV	Lower heating value
BTE	Brake thermal efficiency
HRR	Heat release rate
B_5	5% of biodiesel to 95% of diesel blend
B_{15}	15% of biodiesel to 85% of diesel blend
B_{25}	25% of biodiesel to 75% of diesel blend
B_{100}	100% pure *Khaya senegalensis* biodiesel blend
D_{100}	100% pure diesel blend
m_f	Fuel flow rate
ρ_f, ρ_l	Fuel density
A_n	Nozzle orifice area
C_D	Injector discharge or flow factor
$\Delta\theta$	Injector crank angle
N	Engine speed
N	Swirl speed
S_r	Swirl ratio
ΔP	Pressure differential between the fuel injector side and chamber side
m_a	Air mass flow rate
P_a	Ambient pressure
R	Gas constant, 287 $J.Kg^{-1}K$
T_a	Ambient temperature
H_f	Heat of combustion
d, d_o	Orifice or nozzle diameter
η_c	Combustion efficiency
V_e	Engine capacity
T	Engine torque
T_f	Stack flue temperature
O_m	Stack flue measured O_2
A	Constant, 0.68
O_{21}	21% atmospheric air O_2
K	Dew point heat condensate
B	Constant, 0.007
G_k	Turbulent kinetic energy generated from the velocity gradient
M	RNG turbulence viscosity
K	Turbulent kinetic energy
E	Dissipation energy
$C_{1\varepsilon}$	Model constant, 1.44
$C_{2\varepsilon}$	Model constant, 1.92
C_μ	Turbulent viscosity k-ε constant, 0.09
σ_k	RNG k stress constant, 1.0
σ_ε	RNG ε stress constant, 1.3
$S_{near\text{-}wall}$	Near-wall source term
U	Fuel axial velocity at the injector exit
T	Thickness of the injected film
$\dot{m}_{eff}$	Effective mass flow rate
v_c	Velocity coefficient
d_i	Injector exit diameter
d_l	Diameter of an atomized liquid species
C_l	Levich constant
ħ	Ohnesorge number
ρ_g	Density of gas species
r_c	Smaller child droplet radius
C_{rt}	Breakup radius constant of 0.1
K_{rt}	Wave number